

# Kekulé Superconductivity in Twisted Magic Angle Bilayer Graphene

Ke Wang<sup>1,2</sup> and K. Levin<sup>1</sup>

<sup>1</sup>*Department of Physics and James Franck Institute, University of Chicago, Chicago, Illinois 60637, USA*

<sup>2</sup>*Kadanoff Center for Theoretical Physics, University of Chicago, Chicago, Illinois 60637, USA*

(Dated: October 9, 2025)

Motivated by recent scanning tunneling microscopy experiments which report Kekulé ordering in the twisted graphene family, we develop a microscopic theory of superconductivity, specifically for the bi-layer case. This involves an intra-valley, finite-momentum pair-density wave (PDW) which naturally incorporates a Kekulé distortion into the superconducting phase. The PDW state displays three central features: (i) it spontaneously breaks  $C_3$  rotational symmetry, producing nematic order, and (ii) it possesses a large gap-to-critical-temperature ratio. Moreover, (iii) it yields a quasi-particle density of states having a V-like shape (with a finite value at zero energy) which transitions to a fully gapped, U-shaped spectrum with increasing attraction. These characteristics, including consistency with an allowed Berezinskii-Kosterlitz-Thouless transition, align with key experimental signatures in the twisted graphene family where the U-V transition is observed in the tri-layer case. We find the paired state with a modest interaction strength is near to a BEC-like regime, as appears consistent with the observed extremely short coherence lengths. Together, these results establish a microscopic intra-valley Kekulé PDW state as an essential ingredient towards understanding unconventional superconductivity in twisted graphene.

## INTRODUCTION

It is hard to overestimate the excitement which has been generated by the discovery [1] of “high” temperature superconductivity associated with the flat band regime [2] in twisted bi- and tri-layer graphene [3]. Measured so far are transport properties [4, 5], superfluid density[6, 7], tunneling[8–10], upper critical fields [1, 11], thermodynamical [12] as well as other superconducting characteristics[13–16].

Among these, scanning tunneling spectroscopy and microscopy [17, 18] have led to remarkable progress in understanding the nature of the correlated insulators. What is most notable is evidence for an inter-valley coherent (IVC) ordering, called Kekulé at  $\nu = \pm 2$  and  $\pm 3$  which coincides with a  $\sqrt{3} \times \sqrt{3}$  reconstruction of the atomic scale unit cell. While there has been much theoretical attention paid to the implications for the correlated insulator regimes[17, 18], a form of Kekulé ordering has also been observed within the superconducting and pseudogap phases in the same interval ( $\nu = \pm 2$  to counterpart  $\pm 3$ ). This, we argue here, is essential to address in order to understand the superconductivity in these twisted graphene, flatband systems.

What has been emphasized in the experimental literature is that (i) the superconductor arises out of a Kekulé order that is qualitatively different from that of the neighboring insulator[17], (ii) that the superconducting and pseudogap phases look similar to one another with, thus far, no readily distinguishable features in imaging [17]. (iii) Importantly, the strength of the IVC order, quantified by the normalized Kekulé peak intensity is maximum at filling factors corresponding to those with very strong pairing, as evidenced by the short coherence lengths and the presence of a pseudogap phase[18].

Motivated by this STM data, we now consider intra-valley pairing superconductivity in twisted bilayer graphene (TBG),

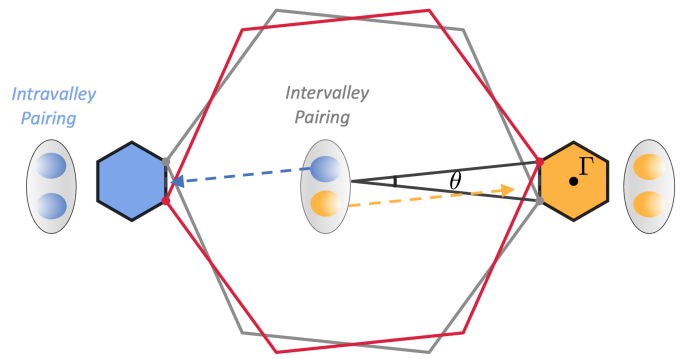


FIG. 1. Cartoon of the twisted bilayer graphene geometry and Cooper Pairs. This serves to contrast intravalley and intervalley pairing. Two graphene Brillouin zones (BZs) are rotated by  $\pm \theta$  (gray/red). Two mini-moiré BZs associated with  $K/K'$  valleys are represented by orange and blue; the  $\Gamma$ -point is shown in the right mini-BZ. Intravalley pairing involves pairs *within* each valley and associated mini-BZ, while intervalley pairing involves two different mini-BZs.

which is a methodology for implementing superconducting Kekulé order [19, 20]. We will see that one can alternatively view this intravalley pairing as a pair density wave (PDW) in which the pairs have non-zero net momentum. In this way, it should be emphasized that “Kekulé superconductivity” as discussed here refers not to a Kekulé pairing mechanism or “glue” but to a Kekulé pairing machinery.

In a qualitative way we can now understand the STM experiments. From (i) it would then appear that one is seeing two distinct Kekulé orders that live in different sectors: in the insulator, a particle-hole Kekulé (bond/charge/valley-coherent) order, and in the superconductor, a particle-particle Kekulé component. From (ii) the observation that pseudogap and superconducting phases show (essentially) the same Kekulé pattern fits naturally with a Kekulé driven pseudogap contain-

ing the same preformed pairs as those that become condensed within the superconducting phase. From (iii) that the highest Kekulé peaks are associated with the strongest pairing seems to strongly support the idea that Kekulé ordering and the superconducting pairing machineries are correlated [21].

This analysis underlines the importance of systematically addressing, as we do here, the intra-valley pairing case which leads to Kekulé superconductivity. This proposal stands in contrast to the majority of current theories, which focus on inter-valley pairing [22–26] (and its variants [27–29]). The simple representation in Figure 1 emphasizes the differences in these two scenarios. One cannot, however, rule out that inter-valley and intra-valley pairing may coexist; they originate from distinct, orthogonal symmetry channels of the underlying microscopic attraction.

We emphasize throughout that this intra-valley pairing scenario leads to important and distinct theoretical consequences from the inter-valley case, some of which are rooted in the structure of the flat-band Bloch wavefunctions. The presence of an effect which we term the “quantum textures” presents a notable contrast. Unlike conventional inter-valley pairing where details about the wavefunction are generally absent from the gap equation, this quantum texture, containing wavefunction information, enters directly into the intra-valley gap equation. It strongly modulates the behavior of the order parameter. We will see the interplay between this texture and the fundamental symmetries of a single moiré valley dictates the nature of the resulting superconducting order. We show how this provides direct microscopic insights into the observed numerical phenomenology.

## PDW ORDER AND MICROSCOPIC MODEL

A pair density wave superconductor [30] involves pairs with finite center-of-mass momentum,  $2\mathbf{Q}$ . The order is bond-centered, forming on the AB/BA sublattice bonds, and in the low-filling regime, *the pairing momentum  $\mathbf{Q}$  is naturally expected to lie near the Dirac point  $\mathbf{K}$* . The full order parameter is a time-reversal-symmetric combination of condensates from the two valleys (e.g.,  $[\Delta_{2\mathbf{Q}}, \Delta_{-2\mathbf{Q}}]$ ).

Another crucial constraint on the nature of this PDW superconductivity comes from the fact that STM experiments cannot probe a PDW directly but rather are sensitive to its consequences through the charge sector which must reveal the specific form of Kekulé order. One important consequence of these two-valley PDW states is that they can induce secondary order, involving charge-density waves (CDWs). A CDW arises from the bilinear coupling of the two valley condensates,

$$\rho(\mathbf{r}) \propto \Delta_{2\mathbf{Q}}(\mathbf{r}) \Delta_{-2\mathbf{Q}}^*(\mathbf{r}) + \text{h.c.}, \quad (1)$$

which carries total momentum  $4\mathbf{Q}$ . On the atomic lattice this reduces to a modulation  $\propto \cos(2\mathbf{K}\mathbf{r})$  (since  $3\mathbf{K}$  is a reciprocal vector), yielding a Kekulé  $\sqrt{3} \times \sqrt{3}$  superlattice, i.e., a tripled

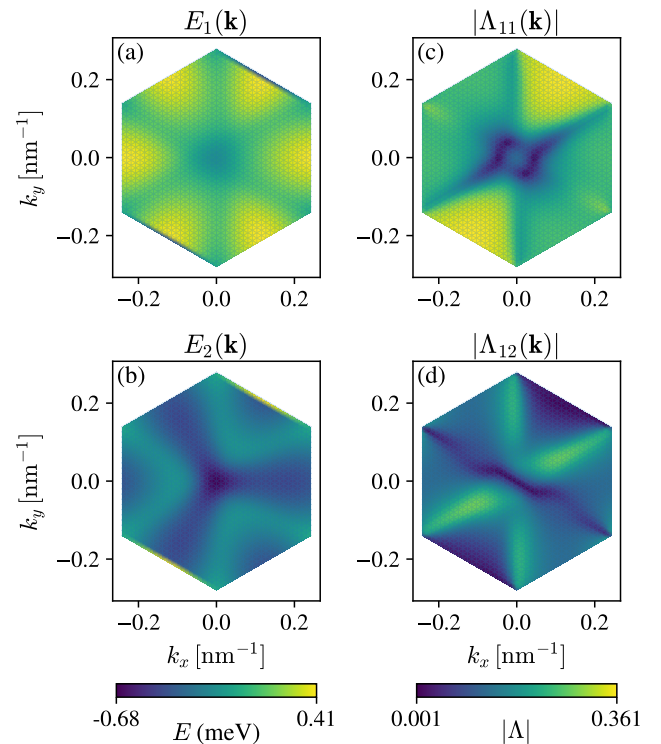


FIG. 2. Flat-band dispersion and form factors from the Bistritzer-MacDonald (BM) model in the mini-Brillouin zone. Parameters:  $w_{AA} = 0.08$  eV,  $w_{AB} = 0.11$  eV, twist angle  $\theta \simeq 0.94$ , and  $\hbar v_F = 0.684$  eV·nm. (a,b) Band energies  $E_1(\mathbf{k})$  and  $E_2(\mathbf{k})$  measured from half-filling; each flat band has bandwidth  $W \approx 0.5$  meV and respects three-fold rotation  $C_3$ . (c,d) Magnitudes of the intra-band and inter-band form factors which enter into the gap equation and are central to the superconductivity. Note in the inter-valley case the form factors are unity which would yield structureless plots.

unit cell. The slowly varying moiré-scale envelope is set by  $\delta\mathbf{q} = 2\mathbf{Q} - 2\mathbf{K}$  and thus varies on the length scale  $|\delta\mathbf{q}|^{-1}$ . Although a full analysis of this secondary order is beyond the scope of this work, this mechanism provides a connection between the proposed PDW and the STM experiments. [31]

Although intra-valley pairing takes place in two different valleys, it is sufficient for our purposes to analyze a single valley separately. That the two valleys contribute independently is well-justified for small twist angles. Our microscopic theory is based on the Bistritzer-MacDonald (BM) continuum model for TBG, supplemented with a short-range attractive interaction. The BM model captures the essential physics of the moiré superlattice through two interlayer tunneling parameters,  $w_{AA}$  and  $w_{AB}$ . A generic translationally invariant pairing interaction can be written as:

$$\hat{V} = \sum V_{aa'}(\mathbf{q} - \mathbf{q}') \psi_{a,\sigma}^\dagger(\mathbf{k}_+) \psi_{a',\sigma'}^\dagger(\mathbf{k}_-) \times \psi_{a',\sigma'}(\mathbf{k}'_-) \psi_{a,\sigma}(\mathbf{k}'_+), \quad (2)$$

where the momenta are defined as  $\mathbf{k}_\pm = \mathbf{k} \pm \mathbf{q}$  and  $\mathbf{k}'_\pm = \mathbf{k}' \pm \mathbf{q}'$ . The summation is over all momenta  $(\mathbf{k}, \mathbf{k}', \mathbf{q}, \mathbf{q}')$ , spin indices  $(\sigma, \sigma')$ , and layer/sublattice indices  $(a, a')$ .

We require pairing interactions to respect all symmetries of the single valley BM model, and involve two different sub-lattices, as we consider AB-bonding order. Among the possible interactions that satisfy these criteria, a natural choice [19, 20] is a nearest-neighbor (NN) attraction within each layer. This is physically motivated by the fact that the interlayer distance is generally larger than the intralayer nearest-neighbor distance.

For definiteness, the numerical results and figures presented throughout this work are based on this NN interaction model. As we will show, the essential properties of the resulting superconducting order originate from the symmetry properties of the BM model. Importantly they are viewed as sufficiently generic and, thus, independent of the details of the assumed short-range attractive interactions.

We begin by utilizing the spatial  $C_3$  rotational symmetry of the lattice to classify the possible superconducting pairing channels. The  $C_3$  point group has three one-dimensional irreducible representations, which we label as  $A$ ,  $E_1$ , and  $E_2$ . An eigenstate belonging to one of these irreducible representations acquires a phase of  $\zeta^l$ ,  $l = 0, 1, 2$  under a  $C_3$  rotation, where  $\zeta = \exp(i2\pi/3)$ . The interaction potential can be decomposed into these eigenstates. For the nearest neighbor model, we have the decomposition for each layer:

$$V(\mathbf{q} - \mathbf{q}') = \sum_{l=0}^2 g_l f_l(\mathbf{q}) f_l^*(\mathbf{q}'). \quad (3)$$

Here  $f_l(\mathbf{q}) = 3^{-1} \sum_{j=0}^2 \zeta^{jl} \exp -i\mathbf{q} \cdot \boldsymbol{\delta}_j$ , and  $\boldsymbol{\delta}_j$  represents the nearest-neighbor vectors in honeycomb lattice.

As shown in Figure 1, for intra-valley pairing, Cooper pairs are formed by electrons within the same moiré valley. As the mini-Brillouin zone is so tiny, this implies that the interaction is dominated by small momentum transfers,  $\mathbf{q}$ . Consequently, the phase factor in each  $f$  is small [32]  $|\mathbf{q} \cdot \boldsymbol{\delta}_j| \ll 1$ . In this limit, the form factor for the  $A$ -channel ( $l = 0$ ) approaches  $f_0(\mathbf{q}) \rightarrow 1$ , while the form factors for the chiral channels ( $l = 1, 2$ ) vanish:  $f_{1,2}(\mathbf{q}) \rightarrow 0$ . Thus the dominant superconducting channel corresponds to  $A$ . [33]

## ORDER PARAMETER AND QUANTUM TEXTURES

For this case which we consider throughout the paper, the pairing gap parameter satisfies:

$$\Delta_{aa',\sigma\sigma'}(\mathbf{Q}) = - \sum_{\mathbf{q}} V_0(\mathbf{q}) \langle \hat{\psi}_{a',\sigma'}(\mathbf{Q}_-) \hat{\psi}_{a,\sigma}(\mathbf{Q}_+) \rangle. \quad (4)$$

Here  $V_0(\mathbf{q}) = g_0 f_0^*(\mathbf{q})$  and  $\mathbf{Q}_{\pm} = \mathbf{Q} \pm \mathbf{q}$ . In the NN model, we have the layer/sublattice indices  $a = LA$  and  $a' = LB$ . This is consistent with the physics of a condensate which forms on the AB sublattice bonds within each layer. Furthermore, the condensates in the two layers are related by mirror symmetry such that they are equal in magnitude.

To analyze the pairing further, we rewrite the order parameter in the spectral (or band) basis. The transformation from

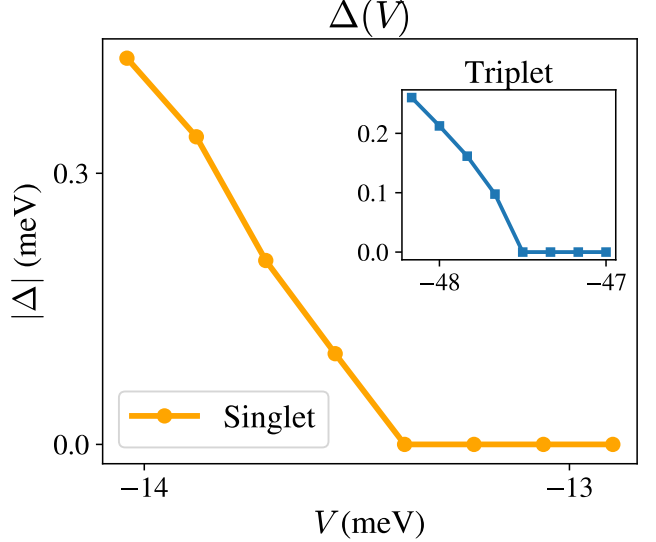


FIG. 3. Singlet/triplet order parameter as a function of interaction strength  $V \equiv V_0(q = 0)$  near zero temperature  $T = 0.01$  meV. The filling is taken to be  $3/8$  of the lower flat band. Singlet pairs need critical coupling  $V_c \sim 10$  meV to support a non-zero order parameter, while triplet pairs need  $V_c \sim 50$  meV. This is due to the different nature of the form factors. Thus we can assume that the superconductivity has singlet order.

the plane-wave basis (operators  $\hat{\psi}$ ) to the spectral basis (operators  $c$ ) requires the introduction of the Bloch wavefunctions,  $u_{\mathbf{G},a;n}(\mathbf{k})$ :

$$\hat{\psi}_{a,\sigma}(\mathbf{k} + \mathbf{G}) = \sum_n u_{\mathbf{G},a;n}(\mathbf{k}) \hat{c}_{n,\sigma}(\mathbf{k}) \quad (5)$$

This leads to the important definition of a (particle-particle) form factor,  $\Lambda_{mn,aa'}(\mathbf{k}, \mathbf{q})$ , which projects the interaction onto the particle-particle channel in this bandstructure basis:

$$\Lambda_{mn,aa'} = \sum_{\mathbf{G}} f_0^*(\mathbf{q} + \mathbf{G}) u_{\mathbf{G},a;m}(\mathbf{Q}_+) u_{-\mathbf{G},a';n}(\mathbf{Q}_-). \quad (6)$$

Using this form factor, Eq. 4 can be rewritten in terms of:

$$\Delta_{aa',\sigma\sigma'} = g_0 \sum_m \Lambda_{mn}(\mathbf{Q}, \mathbf{q}) \langle \hat{c}_{m,\sigma}(\mathbf{Q}_+) \hat{c}_{n,\sigma'}(\mathbf{Q}_-) \rangle. \quad (7)$$

Here the summation is over the band index  $m/n$  and momentum  $\mathbf{q}$  in mini-BZ. We emphasize that in the form factor of Eq. 6, only direct *products* of Bloch wavefunctions appear. This is to be contrasted with their *inner products* which would appear in the particle-hole sector. Time-reversal symmetry relates opposite valleys and is absent within a single moiré valley. Consequently, the diagonal form factor  $\Lambda_{nn}(\mathbf{q} = 0)$  is different from unity, and in practice is often much smaller (as is addressed more explicitly in Fig. 2). This is a key distinction between intra-valley pairing and BCS-like inter-valley pairing (or the correlated Kekulé insulator), where the analogue diagonal form factors are close to unity and effectively play no role.

In our numerical simulations, we adopt the isolated flat-band approximation, which depends on the energy separation parameter  $E_{\text{band}}$  between the flat and remote bands. In this regime, this parameter and the bandwidth  $W$  (which is very small in the absence of strain) satisfy  $\Delta/E_{\text{band}} \ll W/\Delta$ . This is discussed in more detail in the Methods section. Within this flat band scenario, the pairing physics is governed by a form factor matrix,  $\Lambda_{mn}$ , where the indices  $m, n$  span the flat-band basis. We refer to this matrix as a “quantum texture”, and show it plays a central role here. It encodes the momentum-space structure of the pairing interaction and determines the fundamental properties of the condensate.

Our analysis, based on this flat-band projection, has four important implications for the Kekulé superconductor: (1) The system strongly favors *singlet over triplet pairing*; this is derived from the  $C_2\mathcal{T}$  symmetry of the model. (2) The ratio of the zero-temperature gap to the critical temperature is *large* ( $\Delta/T_c \gg 2$ ). (3) The Bogoliubov quasiparticle spectrum spontaneously breaks  $C_3$  rotational symmetry, indicating an *intrinsically nematic* superconducting state[34]. (4) The quasi-particle density of states, as measured in tunneling, has a V-like shape (with a “zero bias conductance”) while it transitions to a fully gapped, U-shaped spectrum with increasing attraction.

### (1) Singlet Pairing and $C_2\mathcal{T}$ -symmetry

We show that the system is more likely to favor singlet than triplet intravalley pairing. As observed in Fig. 3, the coupling required to support singlet superconductivity is substantially smaller than that for the triplet channel. We can understand this numerical finding by demonstrating that it originates from the difference between the form factors in the singlet and triplet channels. This, in turn, derives from the  $C_2\mathcal{T}$  symmetry of the BM model.

We identify the form factors in each spin (singlet- $s$  and triplet- $t$ ) channel:

$$\Lambda^{s/t}(\mathbf{k}, \mathbf{q}) = \Lambda(\mathbf{k}, \mathbf{q}) \pm \Lambda^T(\mathbf{k}, -\mathbf{q}). \quad (8)$$

Here the transpose acts on band indices. From the definition of the order parameter in Eq. 7, one sees that the form factor  $\Lambda$  together with the coupling  $g_0$  plays the role of an effective interaction. Thus, the mini-Brillouin-zone (mBZ) average of  $|\Lambda^{s/t}(\mathbf{0}, \mathbf{q})|$  provides an indicator of which spin channel is favored. Numerically, we confirm that  $\langle |\Lambda^s(\mathbf{0}, \mathbf{q})| \rangle_{\text{mBZ}} > \langle |\Lambda^t(\mathbf{0}, \mathbf{q})| \rangle_{\text{mBZ}}$ . Here  $|\cdot|$  denotes the Frobenius norm of the form-factor matrix in the flat-band subspace, and  $\langle \cdot \rangle_{\text{mBZ}}$  denotes averaging over the mBZ.

This inequality involving the singlet, triplet states follows from the  $C_2\mathcal{T}$  symmetry of TBG. To see what this symmetry implies, we consider a toy model consisting of a nondegenerate two-band system which has  $C_2\mathcal{T}$  symmetry. The model is described by two Bloch functions  $\tilde{u}_{\mathbf{G};n}(\mathbf{k})$  with  $n = 1, 2$ . Under  $C_2\mathcal{T}$ , one has  $\tilde{u}_{\mathbf{G};n}(\mathbf{k}) \rightarrow \tilde{u}_{\mathbf{G};n}^*(\mathbf{k})$ , and in this way the

Bloch functions can be chosen to be real. Such a two-band toy model is used in Ref. [35] to illustrate how symmetry endows the TBG flat bands with an Euler class. The form factor for Cooper pairing in the toy model is given by:

$$\Lambda_{\text{Toy},mn}(\mathbf{Q}, \mathbf{q}) = \sum_{\mathbf{G}} \tilde{u}_{\mathbf{G};m}(\mathbf{Q}_+) \tilde{u}_{-\mathbf{G};n}(\mathbf{Q}_-). \quad (9)$$

This leads to the identity

$$\Lambda_{\text{Toy},mn}(\mathbf{Q}, \mathbf{q}) - \Lambda_{\text{Toy},nm}(\mathbf{Q}, -\mathbf{q}) = 0, \quad (10)$$

and thus the triplet form factor in this toy model *vanishes identically*. This is a direct consequence of the reality of the Bloch functions.

In the more realistic situation, as for TBG,  $C_2\mathcal{T}$  acts as  $\sigma_x\mathcal{K}$  (where  $\mathcal{K}$  implies complex conjugation), and consequently Bloch functions are not strictly real. Thus the triplet form factor does not vanish identically. The symmetry  $C_2\mathcal{T}$  leads to

$$\Lambda_{mn,L}(\mathbf{Q}, \mathbf{q}) \simeq \sum_{\mathbf{G}} u_{\mathbf{G},LA;m}^*(\mathbf{Q}_+) u_{-\mathbf{G},LA;n}(\mathbf{Q}_-). \quad (11)$$

Here we approximate  $f_0(\mathbf{q})$  by  $f_0(0) = 1$  since  $|f_0(\mathbf{q}) - f_0(0)| \ll 1$ . Then with Eq. 11 applied to the triplet state, one sees that the diagonal components of the triplet channel vanish:  $\Lambda_{nn}^t(\mathbf{Q}, \mathbf{q} = \mathbf{0}) = 0$ . This suppression is not found in the singlet channel. This suggests an inequality, quite generally, after averaging over the mBZ  $\langle |\Lambda^s(\mathbf{Q}, \mathbf{q})| \rangle_{\text{mBZ}} > \langle |\Lambda^t(\mathbf{Q}, \mathbf{q})| \rangle_{\text{mBZ}}$ . This inequality then explains the numerical result of Fig. 3 which shows that it takes a much stronger attractive interaction to produce a triplet state.

### (2) Large $\Delta/T_c$ ratio

Solutions of the multiband gap equation show  $\Delta/T_c \sim 10$ , a ratio much larger than the standard BCS value as can be seen from the numerical calculations of Fig. 4. Importantly, we can understand more analytically how this large ratio derives from the properties of the quantum texture. It follows from Figs. 2(c) and (d) that  $|\Lambda_{mn}(\mathbf{q})| < 1$  for all  $\mathbf{q} \in \text{mBZ}$ , and indeed  $|\Lambda_{mn}(\mathbf{q})| \ll 1$  for many values of  $\mathbf{q}$  so that

$$\langle |\Lambda_{mn}(\mathbf{q})|^2 \rangle_{\text{mBZ}} \ll \langle |\Lambda_{mn}(\mathbf{q})| \rangle_{\text{mBZ}} \ll 1. \quad (12)$$

Here,  $m$  and  $n$  refer to the flat-band indices. This inequality reflects the nature of the superconducting order and is a consequence of the facts that (1) the order is located on the AB-bonds, and (2) the condensate in each valley involves only a single moiré valley, which lacks time-reversal and inversion symmetry. (A more detailed discussion of this point is presented in the Methods section.)

To make use of Eq. 12, we consider the gap equation in the simpler case of a *single* flat band, which is appropriate when  $\Lambda_{11} \gg \Lambda_{12}$  and the filling is low. We define  $\varphi(\mathbf{q})$  to be the *single* flat band quantum texture (i.e.,  $|\Lambda_{11}|$ ).

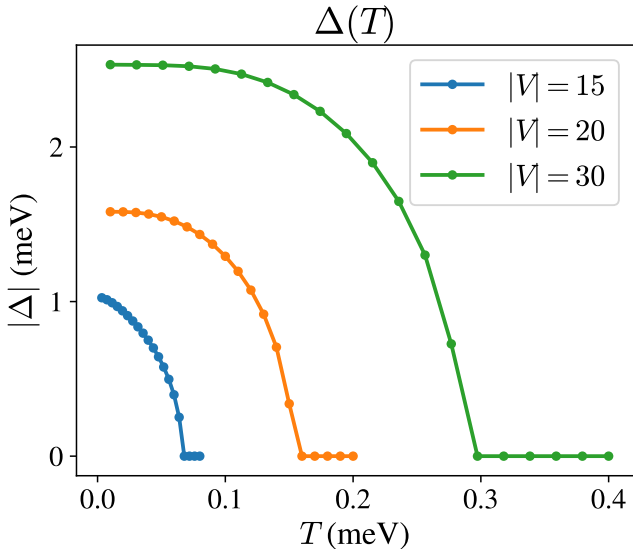


FIG. 4. Temperature dependence of the (singlet) superconducting gap magnitude  $|\Delta(T)|$  for interaction strengths  $V = -15, -20, -30$  meV. The ratios  $\Delta/T_c$  are approximately 14, 10, and 8, i.e., all large, of order 10. The normal-state chemical potential is  $\mu_N = -0.314$  meV. The  $T = 0$  chemical potentials for the three cases are  $\mu = -0.33, -0.38, -0.52$  meV, all well above the band bottom at  $-0.68$  meV; thus, the system is not yet in the BEC regime.

In the flat-band limit ( $W < 2T_c$ ,  $\Delta$ ) where the bandwidth  $W$  is the smallest relevant energy scale in the problem, the gap and  $T_c$  equations take on a rather unfamiliar form. There is a direct proportionality on the pairing interaction, rather than the exponential dependence found in BCS theory. It can be shown that:

$$\Delta \approx \frac{V}{2} \langle \varphi(\mathbf{q}) \rangle_{\text{mBZ}}, \quad T_c \approx \frac{V}{4} \langle \varphi(\mathbf{q})^2 \rangle_{\text{mBZ}}.$$

The ratio  $\Delta/T_c$  is therefore given by:

$$\frac{\Delta}{T_c} \approx 2 \frac{\langle \varphi(\mathbf{q}) \rangle_{\text{mBZ}}}{\langle \varphi(\mathbf{q})^2 \rangle_{\text{mBZ}}}. \quad (13)$$

and from Eq. (12) this leads to  $\Delta/T_c \gg 1$ . In particular, for a system with the parameters shown in Fig. 2, we find  $\langle \varphi(\mathbf{q}) \rangle_{\text{mBZ}} \simeq 0.24$  and  $\langle \varphi(\mathbf{q})^2 \rangle_{\text{mBZ}} \simeq 0.063$ . This yields the relations  $V/\Delta \sim 10$  and  $\Delta/T_c \sim 10$ , which is consistent the findings in Fig. 4.

In the Methods section we investigate the intermediate bandwidth regime showing that the value of this ratio remains large, approximately 10, for the same parameter set as is a consequence of these texture effects which lead to the inequality in Eq. (12).

### (3) Nematic Nature of Superconducting order

The superconducting order under consideration is *generically nematic*, spontaneously breaking the three-fold

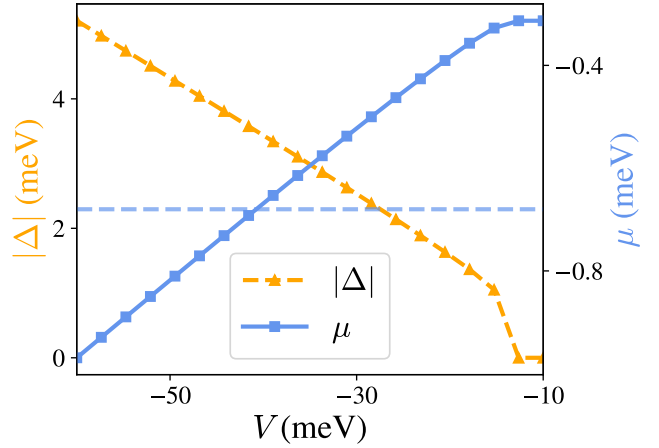


FIG. 5. Order-parameter amplitude  $|\Delta|$  (left axis) and chemical potential  $\mu$  (right axis) versus coupling strength  $V$ . The dashed line marks the flat-band bottom. For attractive  $V \approx 40$  meV (about three times the onset  $V_c$ ), the system crosses into the BEC-like regime.

rotational symmetry  $C_3$ . This can be directly observed in the quantum texture in Fig. 2(c),(d). This anisotropy does *not* originate through a pre-determined pairing interaction, but rather the  $C_3$  rotational symmetry is broken as a consequence of condensation.

Note that this is different from the inter-valley case, where nematicity will emerge after selecting a particular combination of the  $E$ -doublet channels  $f_1/f_2$ . A rigorous proof for the intra-valley case is provided in the Methods section. This proof establishes the fact that in the BM bandstructure, there is a  $C_3$  rotational symmetry about the  $\Gamma$  point of the mini-BZ, but the condensed state is not invariant under a  $C_3$  rotation. Hence there is spontaneous symmetry breaking (SSB) of  $C_3$  symmetry.

In the Methods section we show how this happens by noting that a  $C_3$  rotation essentially causes a momentum boost to the Bloch wavefunction. Equivalently, one can see that there is a unitary operator satisfying

$$U_{C_3}(\mathbf{r}) H(\mathbf{r}) U_{C_3}(\mathbf{r})^\dagger = H(C_3^{-1}\mathbf{r}), \quad (14)$$

where  $U_{C_3}(\mathbf{r}) \sim \exp(i\mathbf{p}_L \cdot \mathbf{r})$  and  $\mathbf{p}_L$  is a layer-dependent momentum. This boost necessarily changes the pairing operator  $\hat{\Delta}(\mathbf{r})$  and shifts the momentum of the condensate,  $\mathbf{Q}$ , to  $\mathbf{Q} + \mathbf{p}_L$ .

### (4) U to V-like transitions in tunneling

In the trilayer case, where Kekulé superconductivity is similarly observed [18] the evolution of the conductance with doping is of particular interest. The tunneling spectrum which reflects the quasi-particle density of states [36], has a V-like shape (often with a “zero bias conductance”) when filling is in the regime closer to  $\nu = -3$ , while it transitions to a U-shaped spectrum, when  $\nu$  is nearer  $-0.2$ . It is generally believed that

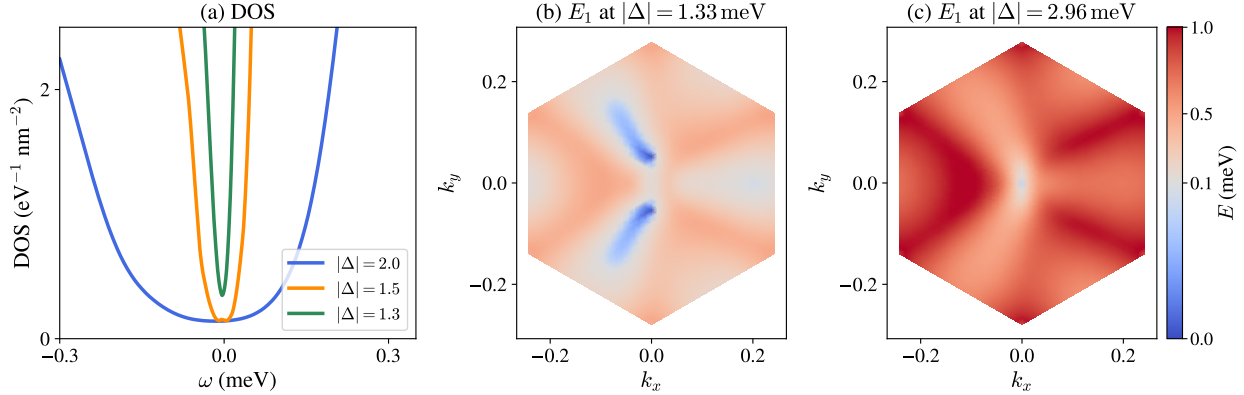


FIG. 6. (a) Figures show the density of states (DOS) versus energy  $\omega$  (meV) for four different gap amplitudes, with curve labels  $|\Delta| \simeq 2.0, 1.5, 1.3$  meV. As the order parameter is reduced, the bottom of the characteristic U-shaped gap narrows towards a V-shape. Note that there is a finite zero bias conductance for the latter case. In (b) we plot the *lowest positive* Bogoliubov deGennes eigenvalue within the mini-Brillouin zone for two values of the order parameter. This demonstrates that for sufficiently small  $\Delta$ , a small Bogoliubov Fermi surface appears and the (V-shaped) DOS spectrum becomes gapless. (c). For larger  $\Delta$  (still away from the BEC regime), the (U-shaped) spectrum is fully gapped.

these spectra, then, reflect a transition from a gapped superconductor to a nodal superconductor. Important to this analysis, one can associate the U regime with a shorter Landau Ginsberg coherence length which reflects [37] stronger attractive interactions. In this vein, while originally this U transition was speculated to relate to a transition all the way to a BEC regime, this has since been effectively refuted [38].

Although these experiments address the tri-layer case, it is useful here to study the density of states (DOS) for our two-flat-band model, using the parameter set corresponding to Fig. 2. As shown in Fig. 6(a), for a superconducting order parameter of  $|\Delta| \geq 1.5$  meV, the DOS exhibits a clear U-shape, indicating that the quasiparticle excitations are fully gapped.

As the order parameter is reduced, the flat bottom of this U-shaped gap narrows, eventually transitioning into a smoothed V-shape with a finite DOS at zero frequency. We find this corresponds to the fact that there are touching points leading to a very small Bogoliubov Fermi surface contained within the quasi-particle dispersions for the “V case” and missing for the “U case”, as can be seen in Fig. 6(b) and Fig. 6(c) [39]. Also important, there is generally a finite conductance at zero energy (zero bias conductance) when the V shape is present. This constitutes a prediction from the present theory.

We can show that the V-like regime originates from the (very minimal) lack of inversion symmetry ( $\mathbf{q} \rightarrow -\mathbf{q}$ ) in the Bistritzer–MacDonald model for a single valley bandstructure. While the U shaped spectrum reflects the fact that the singlet form factor is nodeless, More precisely it is useful to consider the Bogoliubov dispersion in the single flat-band limit:

$$E(\mathbf{q}) = \delta\epsilon(\mathbf{q}) \pm \sqrt{\bar{\epsilon}(\mathbf{q})^2 + \Delta^2\varphi(\mathbf{q})^2}$$

where  $\delta\epsilon(\mathbf{q}) = [\epsilon(\mathbf{q}) - \epsilon(-\mathbf{q})]/2$  and  $\bar{\epsilon}(\mathbf{q}) = [\epsilon(\mathbf{q}) + \epsilon(-\mathbf{q})]/2$  are derived from the dispersion of the partially filled flat band,

$\epsilon(\mathbf{q})$ . Here  $\delta\epsilon(\mathbf{q})$  reflects the lack of inversion symmetry.

From this expression, two regimes emerge. When  $\Delta$  is large enough such that the condition  $|\Delta\varphi(\mathbf{q})| > |\delta\epsilon(\mathbf{q})|$  holds for all  $\mathbf{q}$ , the dispersion is necessarily gapped, leading to the U-shaped DOS. Conversely, when  $\Delta$  is small enough that  $|\Delta\varphi(\mathbf{q})| \leq |\delta\epsilon(\mathbf{q})|$  for some  $\mathbf{q}$ , gapless points can develop. This results in a V-shaped DOS generally associated with a small Bogoliubov Fermi surface, reflecting the sharpness of the V. We anticipate the existence of a critical value,  $\Delta_c$ , that marks a transition from a fully gapped to a gapless superconducting state.

*Experimental Tests: Zero-bias Conductance.* These observations lead to a very simple self consistency test of the theory. We consider a plot of the zero bias conductance as a function of temperature as compared with the temperature dependence of order parameter  $\Delta$ . This is shown in Fig. 7 and is inspired by a related plot (see their Fig 3e) for the moiré materials in Ref. [40]. One can speculate that here the V-shaped tunneling spectra may be qualitatively different from the classic  $d$ -wave behavior in the cuprates [41] where a plot  $dI/dV \propto V$  vanishes exactly at zero bias. Throughout the cuprate family, however, there are some indications of a finite zero bias conductance but these are generally understood [42] as associated with a Dynes lifetime parameter in the tunneling density of states. What is different about the moiré systems, is that the finite zero-bias conductance appears order-parameter controlled, not merely lifetime-broadened. This suggests a superconducting state whose excitation spectrum remains partially gapless due to intrinsic features of the paired state itself, as illustrated in Fig. 7. Here this reflects the presence of an (albeit tiny) Bogoliubov Fermi surface.

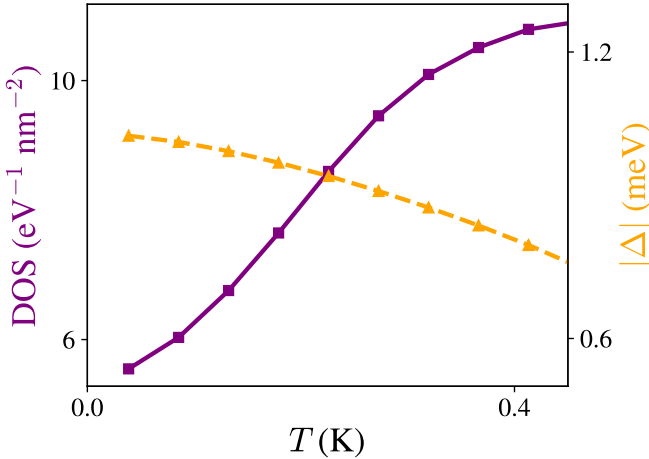


FIG. 7. Density of states and order parameter versus temperature, computed at the interaction strength  $V = 15\text{meV}$ . As temperature increases, the order parameter decreases while the DOS increases. This behavior is consistent with the presence of a Bogoliubov Fermi surface and can be seen to be related to Figure 3e in Ref. [40] (see text), which addresses the zero-bias conductance.

## CONCLUSIONS

We have three central results concerning the twisted graphene family in this paper which we argue have some support from experiment: these are nematic order[34], U to V transitions[36] and large gap to  $T_c$  ratios[9]. All these results are generic consequences of Kekulé superconducting order and symmetry properties of the single moiré valley (BM) model. At the heart of our paper is the assumption of intra-valley (Kekulé) pairing in which the major support comes from an observed correlation [18] in these moiré systems between the highest Kekulé peaks which are associated with the strongest pairing regime.

We argue against the interpretation that Kekulé order acts as a pairing "glue" since we know in superconductors which have a non-phononic, bosonic (e.g., magnetic) pairing mechanism, the superconductivity is strongest when the non-superconducting, alternative ordering is weakest[43]. Rather Kekulé order seems to be intertwined with the pairing machinery as distinct from the pairing mechanism. This order then leads to a PDW-like description of the superconductivity[19, 20, 44].

We have, throughout this paper, made few distinctions between the bi- and tri-layer moiré graphene superconductors. We believe, in line with most of the experimental phenomenology, that many of the general features discussed here apply to both; we focus almost exclusively on the physics of the two flat bands and the related symmetries. There is an interesting distinction however which is that the attractive interactions (as measured by the large size of the pairing gap and the very short Landau Ginsberg coherence lengths) may not be strong enough in the bilayer case to reveal a U shaped

tunneling spectra. The V shape features should remain and it would be important to see if there is consistency with the theoretically expected trends which associate this regime with a finite zero bias conductance.

In summary, it is our contention in this paper that this Kekulé/PDW form of superconductivity is an essential ingredient which must be included in order to ultimately understand superconductivity in the twisted graphene family.

## Methods

### Bistritzer–MacDonald Model and Symmetries

We briefly review the Bistritzer–MacDonald (BM) model of twisted bilayer graphene (TBG) and its symmetries. When two layers are stacked with a relative twist angle  $\theta$ , a fundamental momentum scale emerges,

$$k_\theta = 2K \sin \frac{\theta}{2}, \quad K = \frac{4\pi}{3\sqrt{3}a}, \quad (15)$$

where  $a$  is the graphene lattice constant. A convenient choice of momentum difference between the two Dirac points is

$$\mathbf{q}_1 = \mathbf{K}_{\text{top}} - \mathbf{K}_{\text{bot}} = (0, 1) k_\theta. \quad (16)$$

The remaining moiré reciprocal vectors can be defined as  $\mathbf{b}_{1,2} = \mathbf{q}_{2,3} - \mathbf{q}_1$ , where  $\mathbf{q}_{2,3}$  are obtained by counterclockwise rotations of  $\mathbf{q}_1$  by  $120^\circ$ .

The BM Hamiltonian describes the continuum theory near the two Dirac cones,

$$H = v \left( -i\nabla - \frac{\tau_z}{2} \mathbf{q}_1 + \mathbf{M} \right) \cdot \boldsymbol{\sigma}_{\theta/2} + [T(\mathbf{r})\tau^+ + \text{h.c.}], \quad (17)$$

where  $v$  is the Fermi velocity of monolayer graphene,  $\mathbf{M}$  denotes the  $M$ -point of the mini Brillouin zone,  $\tau$  and  $\sigma$  act on layer and sublattice indices, and  $\boldsymbol{\sigma}_{\pm\theta/2}$  denote Pauli matrices rotated by angle  $\pm\theta/2$ . The tunneling matrix  $T(\mathbf{r})$  is parameterized by two amplitudes  $w_{AA}$  and  $w_{AB}$ ,

$$T(\mathbf{r}) = w_{AA} \alpha_0(\mathbf{r}) + w_{AB} \sigma^+ \alpha_1(\mathbf{r}) + w_{AB} \sigma^- \alpha_2(\mathbf{r}), \quad (18)$$

with spatial form factors

$$\alpha_m(\mathbf{r}) = \sum_{j=0}^2 w^{mj} e^{-i\mathbf{b}_j \cdot \mathbf{r}}, \quad b_0 = \mathbf{0}, \quad w = e^{i2\pi/3}. \quad (19)$$

The BM Hamiltonian respects four fundamental symmetries: moiré translations, threefold rotations  $C_3$ , mirror reflection  $M_y$ , and the combined twofold rotation with time reversal  $C_2\mathcal{T}$ . For a spatial transformation  $R$ , the Hamiltonian transforms as

$$H'(\mathbf{x}) = H(R^{-1}\mathbf{x}), \quad (20)$$

and invariance under the symmetry requires

$$H'(\mathbf{x}) = U(\mathbf{x})H(\mathbf{x})U^\dagger(\mathbf{x}), \quad (21)$$

with  $U(\mathbf{x})$  a unitary operator. Explicitly, the mirror symmetry and threefold rotation[45] are represented by  $U_{M_y} = \sigma_x \tau_x$  and

$$U_{C_3}(\mathbf{x}) = \exp\left(\frac{2\pi i}{3} \hat{z} \cdot \boldsymbol{\sigma}\right) \exp\left[i\left(2\mathbf{M} + \mathbf{b}_1 \frac{\tau_z + 1}{2}\right) \cdot \mathbf{x}\right]. \quad (22)$$

For the antiunitary  $C_2\mathcal{T}$  operation, one has

$$H'(\mathbf{x}) = H^*(-\mathbf{x}), \quad H'(\mathbf{x}) = \sigma_x H(\mathbf{x}) \sigma_x, \quad (23)$$

which guarantees invariance under the combined symmetry.

### Flat band Approximation

We find that  $\Lambda$  is highly nonlocal in the band index: sizeable matrix elements  $|\Lambda_{mn}(\mathbf{q})|$  persist even for  $|m - n| \gg 1$ . Thus it is necessary to investigate the coupling between the flat bands and remote bands. Experimental data and numerical simulations consistently indicate a significant separation of energy scales. The superconducting gap is typically on the order of  $\Delta \sim 1$  meV, whereas the single-particle gap separating the flat and remote bands in the BM model is much larger, at  $E_{\text{band}} \sim 50$  meV. A Schrieffer–Wolff transformation can be employed to integrate out the remote bands:

$$\tilde{H}_{LL} \simeq H_{LL} + H_{LH}(-H_{HH})^{-1}H_{HL}. \quad (24)$$

Here,  $H_{LL}$  is the Hamiltonian in the flat-band subspace,  $H_{LH}$  couples the flat and remote bands, and  $H_{HH}$  is the Hamiltonian within the remote-band subspace. After the transformation, the new Hamiltonian  $\tilde{H}_{LL}$  acquires a correction of order  $\Delta^2/E_{\text{band}}$ . When this energy is much smaller than the bandwidth  $W$  of a *single* flat band, the isolated-flat-band description of intra-valley superconductivity is well-justified. By contrast, in perfectly flat bands ( $W \rightarrow 0$ ) or for sufficiently large  $\Delta$ , remote-band effects must be included.

### Quantum Textures

We show that the quantum texture contribution (arising from the BM bandstructure wavefunctions) is strictly smaller than 1, and in practice much smaller. It suffices to analyze the diagonal singlet form factor  $\Lambda_{nn,L}^s(\mathbf{q})$ , since the off-diagonal singlets and all triplet factors are smaller than  $\Lambda_{nn,L}^s$ .

(i) *Sublattice selectivity from AB bonds.* Because the superconducting order we consider is AB-bond-like, the form factor in Eq. 11 involves products of sublattice-polarized components after the  $C_2\mathcal{T}$  transformation; effectively, only half of the wavefunction components contribute. In the nonchiral limit the Bloch states are *not* fully sublattice polarized (their weight is distributed between A and B), and by normalization of the Bloch wavefunction this immediately suppresses  $\Lambda_{nn,L}(\mathbf{q})$  below 1.

(ii) *Lack of inversion in a single valley.* In a single-valley model, the  $\mathbf{q} \rightarrow -\mathbf{q}$  inversion symmetry is absent, so in general  $u_{\mathbf{G},a;n}(\mathbf{q}) \neq u_{-\mathbf{G},a;n}(-\mathbf{q})$ . Since Cooper pairing combines  $(\mathbf{G}, -\mathbf{G})$  harmonics, this asymmetry further reduces the form factor. Define the even/odd combinations

$$f_{\mathbf{G},a;n}^\pm(\mathbf{q}) = \frac{1}{\sqrt{2}} [u_{\mathbf{G},a;n}(\mathbf{q}) \pm u_{-\mathbf{G},a;n}(-\mathbf{q})]. \quad (25)$$

With the inner product  $\langle x|y \rangle \equiv \sum_{\mathbf{G}} x_{\mathbf{G}}^* y_{\mathbf{G}}$ , the diagonal form factor can be written as

$$\Lambda_{nn,L}^s(0, \mathbf{q}) = \langle f_{a,n}^+(\mathbf{q}) | f_{a,n}^+(\mathbf{q}) \rangle - \langle f_{a,n}^-(\mathbf{q}) | f_{a,n}^-(\mathbf{q}) \rangle. \quad (26)$$

If  $u_{\mathbf{G}} \neq u_{-\mathbf{G}}$ , then the “odd” overlap  $\langle f_{a,n}^-(\mathbf{q}) | f_{a,n}^-(\mathbf{q}) \rangle \neq 0$  and subtracts from the “even” overlap, reducing  $|\Lambda_{nn,L}^s|$ .

Consequently,  $\Lambda_{nn,L}^s(\mathbf{q}) < 1$ , and these two effects typically make it *much* smaller than 1.

### A single flat-band Analysis

Solutions of the multiband gap equation show  $\Delta/T_c \sim 10$  where the  $\Delta$  is close to the ground state value (Fig. 4). To understand the origin of this large ratio, we consider superconducting gap for a single flat band. This approximation is justified since the intraband matrix elements of the pairing form factor are much larger than the interband counterparts.

The Bogoliubov-de Gennes (BdG) Hamiltonian for a single flat-band model can be expressed in the Nambu basis as:

$$H_{\text{single}} = \begin{pmatrix} \epsilon(\mathbf{q}) & \varphi(\mathbf{q})\Delta \\ \varphi(\mathbf{q})\Delta & -\epsilon(-\mathbf{q}) \end{pmatrix} \quad (27)$$

Here,  $\epsilon(\mathbf{q})$  represents the dispersion of the partially-filled flat band, and  $\varphi(\mathbf{q})$  is the pairing form factor projected onto this band (i.e.,  $\Lambda_{11}(\mathbf{q})$ ).

The Bogoliubov quasi-particle dispersion is then given by

$$E_{\pm}(\mathbf{q}) = \delta\epsilon(\mathbf{q}) \pm E(\mathbf{q}). \quad (28)$$

where  $\delta\epsilon = [\epsilon(\mathbf{q}) - \epsilon(-\mathbf{q})]/2$  and  $E_{\mathbf{q}} = \sqrt{\epsilon(\mathbf{q})^2 + \Delta^2\varphi(\mathbf{q})^2}$ . In this expression, the  $\delta\epsilon(\mathbf{q})$  term directly reflects the breaking of inversion symmetry, while the radical term,  $\sqrt{\epsilon(\mathbf{q})^2 + \Delta^2\varphi(\mathbf{q})^2}$ , corresponds to the conventional Bogoliubov dispersion found in centrosymmetric superconductors.

In this Methods section, we primarily consider a sufficiently large enough  $\Delta$  such that the quasi-particle dispersion is fully *gapped*. This corresponds to the U-shaped regime in the DOS in Fig. 8. In this limit, we can analyze the gap equation[46]:

$$\frac{1}{V} = \left\langle \frac{\varphi(\mathbf{q})^2}{2E_{\mathbf{q}}} \tanh\left(\frac{E_{\mathbf{q}}}{2T}\right) \right\rangle_{\text{mBZ}}, \quad (29)$$

where  $E_{\mathbf{q}} = \sqrt{\epsilon(\mathbf{q})^2 + \Delta^2\varphi(\mathbf{q})^2}$  is the quasiparticle energy and  $\varphi(\mathbf{q})$  is the form factor projected onto the flat band (e.g.,  $\Lambda_{11}(\mathbf{q})$ ).

We consider the zero-temperature limit. In general, the superconducting order parameter  $\Delta$  depends on the interaction

strength  $V = V_0(\mathbf{q} = 0)$ . In the BM model (without strain effects) the bands are extremely flat so that the bandwidth  $W \sim 0.5$  meV. We observe that  $\Delta > W$  is satisfied for most  $V$  associated with a superconducting phase, where consistent with experiment,  $\Delta \sim 1$  meV.

In the limit  $\Delta > W$  the zero-temperature gap can be approximated as

$$\Delta \approx \frac{V}{2} \langle \varphi(\mathbf{q}) \rangle_{\text{mBZ}}.$$

*Narrow-band limit.* In the limit  $2T_c > W$  linearizing Eq. (29) yields

$$T_c \approx \frac{V}{4} \langle \varphi(\mathbf{q})^2 \rangle_{\text{mBZ}}.$$

Combining this with the zero-temperature result gives Eq. 13 in the main-text. This expression holds when the bandwidth  $W$  is the smallest relevant energy scale. The ratio on the right-hand side of Eq. 13 is strictly larger than 2. This can be seen as due to the absence of inversion symmetry in a single valley. For typical parameters, the right-hand side for the single flat-band form factor is  $\approx 7.8$ , if we let  $\varphi(\mathbf{q}) = \Lambda_{11,L}(\mathbf{Q} = \Gamma, \mathbf{q})$ , close to the numerically observed ratio for  $\Delta/T_c$ .

*Small  $T_c$  limit.* In the regime  $T_c \ll W$  and at low filling ( $\mu \ll W$ ), the factor  $\tanh(\epsilon/2T_c)$  is sensitive to  $T_c$  only for  $|\epsilon| \sim T_c$ ; otherwise  $\tanh(\epsilon/2T_c) \approx \pm 1$ . Since  $T_c/W \ll 1$ , only a narrow energy window near the Fermi level is relevant for determining  $T_c$ . Accordingly, we approximate the dispersion near the Fermi level. Because we are at low filling, an expansion about the band bottom is appropriate:  $\epsilon(\mathbf{q}) \simeq q^2/2M - \mu$ , where  $M$  is the effective mass obtained by expanding around the band minimum. In two dimensions this implies  $d^2q = M d\epsilon d\theta$ . Numerically,  $\varphi(\mathbf{q})$  saturates rapidly with  $|\mathbf{q}|$ , and we approximate it as angle-only,  $\varphi(\mathbf{q}) \rightarrow \varphi(\theta)$ .

The linearized ( $\Delta \rightarrow 0$ ) gap equation becomes

$$\frac{1}{V} \simeq \langle \varphi(\theta)^2 \rangle_{\text{mBZ}} \frac{1}{W} \int_0^W d\epsilon \frac{1}{2\epsilon} \tanh\left(\frac{\epsilon}{2T_c}\right). \quad (30)$$

Using the standard asymptotic

$$\int_0^W \frac{d\epsilon}{\epsilon} \tanh\left(\frac{\epsilon}{2T_c}\right) = \ln\left(\frac{cW}{T_c}\right), \quad (31)$$

with  $c \approx 1.13$ , Eq. (30) gives

$$T_c \simeq cW \exp\left[-\frac{2W}{V\langle \varphi^2 \rangle_{\text{mBZ}}}\right]. \quad (32)$$

Using the zero temperature result of order parameter, one finds

$$\frac{\Delta}{T_c} \simeq \frac{V}{2cW} \langle \varphi \rangle_{\text{mBZ}} \exp\left[\frac{2W}{V\langle \varphi^2 \rangle_{\text{mBZ}}}\right]. \quad (33)$$

We use typical parameters:  $V = 10$  meV,  $\langle \varphi \rangle_{\text{mBZ}} = 0.24$ ,  $\langle \varphi^2 \rangle_{\text{mBZ}} = 0.063$ ,  $W = 0.5$  meV, and Eq. 33 is evaluated to be  $\Delta/T_c \simeq 10$ .

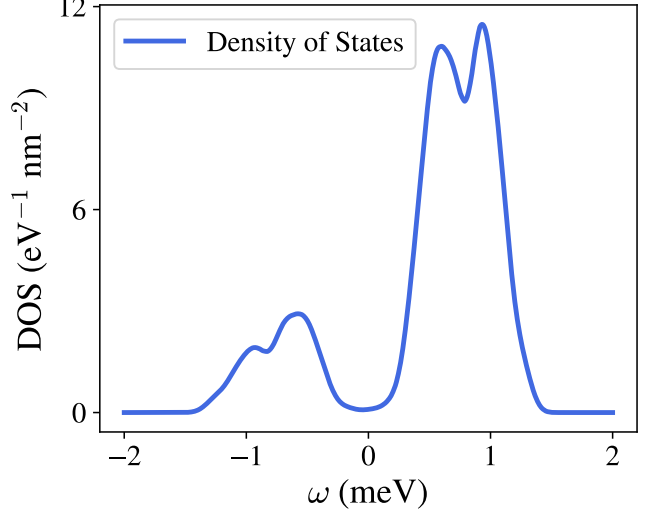


FIG. 8. U-shaped density of states (DOS) from two-flat-band superconductivity. The figure is plotted at  $|\Delta| \simeq 2.5$  meV. From the DOS, the coherence peak appears at  $\omega = \Delta_t \simeq 1$  meV, which is smaller than the order parameter  $|\Delta|$ . The dip feature around  $\omega \sim 1$  meV originates from the band touching of two BM flat bands at  $K/K'$  points.

### U/V-transitions in the DOS

As discussed in the main text, the U/V transition can be understood through the single-band analysis presented in Eq. (28). For a typical order parameter, say  $\Delta \sim 1$  meV, the associated Bogoliubov Fermi surface is small, as depicted in Fig. 6. This originates from the condition  $\delta\epsilon/W \ll 1$ , which indicates that the inversion symmetry breaking is quite weak. Consequently the “V” shape has a rather sharp minimum.

Here, we present the full plot of the density of states (DOS) within the U-shaped regime in Fig. 8. While the low-energy behavior has already been presented, substructure corresponding to dips are observable around  $\omega \sim 1$  meV. These dips arise from the structure of two flat bands that touch at the  $K$  and  $K'$  points. The particle-hole asymmetry in the DOS is a result of our choice of filling which is taken to be  $3/8$  of the lower flat band (equivalent to  $\nu = -2.5$  filling in experiments).

Additionally, the energy scale of the coherence-peaks,  $\Delta_t$ , can be extracted from the DOS. We find that it is smaller than the order parameter, and satisfies  $\Delta_t/\Delta \approx 0.4 < 1$ . Noteably, although the ratio  $2\Delta_t/T_c$  is smaller than  $2\Delta/T_c$ , it remains significantly larger than the weak-coupling BCS value.

### Proof of $C_3$ -SSB

Here we provide a proof that the intravalley superconducting order breaks  $C_3$ -symmetry. In the BM model, there is a  $C_3$  symmetry about  $\Gamma$ . A counterclockwise  $C_3$  rotation is represented by the unitary operator in Eq. 22.

The action of  $U_{C_3}$  on the pairing operator  $\hat{\Delta}(\mathbf{r})$  induces a layer-dependent momentum boost:

$$\hat{\Delta}_{L,\sigma\sigma'}(\mathbf{r}) \longmapsto e^{2i\mathbf{P}_L \cdot \mathbf{r}} \hat{\Delta}_{L,\sigma\sigma'}(\mathbf{r}). \quad (34)$$

Here  $\hat{\Delta}(\mathbf{r})$  denotes the operator corresponding to Eq. (4), and only the layer index  $L$  is preserved for simplicity, and  $\mathbf{P}_L = 2\mathbf{M}$  for the bottom layer while  $\mathbf{P}_L = 2\mathbf{M} + \mathbf{b}_1$  for the top layer. This phase cannot be removed by a global U(1) gauge choice: it is a *layer-dependent* linear function of  $\mathbf{r}$  (a boost), so gauging it away in one layer necessarily induces an incompatible shift in the other.

First consider condensation at the highest-symmetry  $\Gamma$  point of the model and take this as the reference momentum, i.e., the pairing momentum  $\mathbf{Q} = 0$ . Here we examine the symmetry of mean-field Hamiltonian, i.e., fixing condensate and transforming fermions[47]. Since the BM-model term is invariant under a  $C_3$  rotation, we only need to examine the mean-field term:

$$- \sum_{\mathbf{q}, m, n} \Delta_{L,\sigma\sigma'} \Lambda_{mn,L}^*(\mathbf{0}, \mathbf{q}) \hat{c}_{\sigma,m}^\dagger(\mathbf{q}) \hat{c}_{\sigma',n}^\dagger(-\mathbf{q}). \quad (35)$$

A  $C_3$  rotation acts as

$$\Lambda_{mn,L}^*(\mathbf{0}, \mathbf{q}) \longmapsto \Lambda_{mn,L}^*(-\mathbf{P}_L, \mathbf{q}), \quad (36)$$

which shifts the pairs' center-of-mass momentum by  $\mathbf{P}_L$ . Recalling the definition in Eq. 6, the Bloch-amplitude product  $u_{\mathbf{G}} u_{-\mathbf{G}}$  in the form factor becomes  $u_{\mathbf{G}-\mathbf{P}_L} u_{-\mathbf{G}-\mathbf{P}_L}$ , thereby modifying the form factor. Hence the Bogoliubov spectrum is not invariant under  $C_3$ , which is consistent with the form factor presented in Fig. 2.

If the condensate forms at a finite momentum  $\mathbf{k} \neq \Gamma$ ,  $C_3$  is likewise broken:  $\mathbf{k}$  itself rotates under  $C_3$ , and the shift in Eq. (36) still applies. This completes the proof that superconducting order generically breaks threefold rotational symmetry. Importantly, the argument does not rely on any particular form of the attractive interaction; it uses only that the superconducting order is intra-valley.

### Data availability

The data analyzed in the current study are available from the author Ke Wang on reasonable request.

### Code availability

The codes used for the current study are available from the author Ke Wang on reasonable request.

### Acknowledgement

We thank Kevin Nuckolls, Ivar Martin, Bitan Roy, Zhiqiang Wang and Ananth Malladi for helpful discussions. We also acknowledge the University of Chicago's Research Computing Center for their support of this work.

### Author Contributions

K.L. conceived and supervised the project. K.W. performed the computations. K.W. contributed to the acquisition of the data and preparation of figures. All authors have contributed to the interpretation of the data and the drafting as well as the revision of the manuscript.

### Competing Interests

The authors declare no competing interests.

### ADDITIONAL INFORMATION

Correspondence and requests for materials should be addressed to the authors K. Wang and K. Levin.

---

- [1] Y. Cao, V. Fatemi, S. Fang, K. Watanabe, T. Taniguchi, E. Kaxiras, and P. Jarillo-Herrero, Unconventional superconductivity in magic-angle graphene superlattices, *Nature* **556**, 43 (2018).
- [2] R. Bistritzer and A. H. MacDonald, Moiré bands in twisted double-layer graphene, *Proceedings of the National Academy of Sciences* **108**, 12233 (2011).
- [3] K. P. Nuckolls and A. Yazdani, A microscopic perspective on moiré materials, *Nature Reviews Materials* **9**, 460 (2024).
- [4] H. Polshyn, M. Yankowitz, S. Chen, Y. Zhang, K. Watanabe, T. Taniguchi, C. R. Dean, and A. F. Young, Large linear-in-temperature resistivity in twisted bilayer graphene, *Nature Physics* **15**, 1011 (2019).
- [5] Y. Cao, D. Chowdhury, D. Rodan-Legrain, O. Rubies-Bigorda, K. Watanabe, T. Taniguchi, T. Senthil, and P. Jarillo-Herrero, Strange metal in magic-angle graphene with near planckian dissipation, *Phys. Rev. Lett.* **124**, 076801 (2020).
- [6] A. Banerjee, Z. Hao, M. Kreidel, P. Ledwith, I. Phinney, J. M. Park, A. Zimmerman, M. E. Wesson, K. Watanabe, T. Taniguchi, *et al.*, Superfluid stiffness of twisted trilayer graphene superconductors, *Nature* **638**, 93 (2025).
- [7] M. Tanaka, J. L.-j. Wang, T. H. Dinh, D. Rodan-Legrain, S. Zaman, M. Hays, A. Almanakly, B. Kannan, D. K. Kim, B. M. Niedzielski, *et al.*, Superfluid stiffness of magic-angle twisted bilayer graphene, *Nature* **638**, 99 (2025).
- [8] Y. Jiang, X. Lai, K. Watanabe, T. Taniguchi, K. Haule, J. Mao, and E. Y. Andrei, Charge order and broken rotational symmetry in magic-angle twisted bilayer graphene, *Nature* **573**, 91 (2019).
- [9] M. Oh, K. P. Nuckolls, D. Wong, R. L. Lee, X. Liu, K. Watanabe, T. Taniguchi, and A. Yazdani, Evidence for unconventional superconductivity in twisted bilayer graphene, *Nature* **600**, 240 (2021).
- [10] Y. Xie, B. Lian, B. Jäck, X. Liu, C.-L. Chiu, K. Watanabe, T. Taniguchi, B. A. Bernevig, and A. Yazdani, Spectroscopic signatures of many-body correlations in magic-angle twisted bilayer graphene, *Nature* **572**, 101 (2019).
- [11] J. M. Park, Y. Cao, K. Watanabe, T. Taniguchi, and P. Jarillo-Herrero, Tunable strongly coupled superconductivity in magic-angle twisted trilayer graphene, *Nature* **590**, 249 (2021).

[12] U. Zondiner, A. Rozen, D. Rodan-Legrain, Y. Cao, R. Queiroz, T. Taniguchi, K. Watanabe, Y. Oreg, F. von Oppen, A. Stern, *et al.*, Cascade of phase transitions and dirac revivals in magic-angle graphene, *Nature* **582**, 203 (2020).

[13] M. Yankowitz, S. W. Chen, H. Polshyn, Y. X. Zhang, K. Watanabe, T. Taniguchi, D. Graf, A. F. Young, and C. R. Dean, Tuning superconductivity in twisted bilayer graphene, *Science* **363**, 1059 (2019).

[14] A. L. Sharpe, E. J. Fox, A. W. Barnard, J. Finney, K. Watanabe, T. Taniguchi, M. A. Kastner, and D. Goldhaber-Gordon, Emergent ferromagnetism near three-quarters filling in twisted bilayer graphene, *Science* **365**, 605 (2019).

[15] P. Stepanov, I. Das, X. Lu, A. Fahimniya, K. Watanabe, T. Taniguchi, F. H. Koppens, J. Lischner, L. Levitov, and D. K. Efetov, The interplay of insulating and superconducting orders in magic-angle graphene bilayers, [arXiv:1911.09198](https://arxiv.org/abs/1911.09198) (2019).

[16] Y. Saito, J. Ge, K. Watanabe, T. Taniguchi, and A. F. Young, Decoupling superconductivity and correlated insulators in twisted bilayer graphene, [arXiv:1911.13302](https://arxiv.org/abs/1911.13302) (2019).

[17] K. P. Nuckolls, R. L. Lee, M. Oh, D. Wong, T. Soejima, J. P. Hong, D. Călugăru, J. Herzog-Arbeitman, B. A. Bernevig, K. Watanabe, *et al.*, Quantum textures of the many-body wavefunctions in magic-angle graphene, *Nature* **620**, 525 (2023).

[18] H. Kim, Y. Choi, É. Lantagne-Hurtubise, C. Lewandowski, A. Thomson, L. Kong, H. Zhou, E. Baum, Y. Zhang, L. Holleis, *et al.*, Imaging inter-valley coherent order in magic-angle twisted trilayer graphene, *Nature* **623**, 942 (2023).

[19] S. Tsuchiya, J. Goryo, E. Arahata, and M. Sigrist, Cooperon condensation and intravalley pairing states in honeycomb dirac systems, *Physical Review B* **94**, 104508 (2016).

[20] B. Roy and I. F. Herbut, Unconventional superconductivity on honeycomb lattice: Theory of kekulé order parameter, *Phys. Rev. B* **82**, 035429 (2010).

[21] To be precise, this correlation should not be viewed as a “Kekulé-driven pairing mechanism”. As shown in arXiv:2506.18996, quite generally, the strongest pairing tends to occur where the non-superconducting ordering (in this case, Kekulé) is weakest, as in a quantum-critical-point scenario and also more generally.

[22] Y.-Z. You and A. Vishwanath, Superconductivity from valley fluctuations and approximate so (4) symmetry in a weak coupling theory of twisted bilayer graphene, *npj Quantum Materials* **4**, 16 (2019).

[23] F. Wu, A. H. MacDonald, and I. Martin, Theory of phonon-mediated superconductivity in twisted bilayer graphene, *Physical review letters* **121**, 257001 (2018).

[24] B. Lian, Z. Wang, and B. A. Bernevig, Twisted bilayer graphene: a phonon-driven superconductor, *Physical review letters* **122**, 257002 (2019).

[25] T. Cea and F. Guinea, Coulomb interaction, phonons, and superconductivity in twisted bilayer graphene, *Proceedings of the National Academy of Sciences* **118**, e2107874118 (2021).

[26] M. Christos, S. Sachdev, and M. S. Scheurer, Nodal band-off-diagonal superconductivity in twisted graphene superlattices, *Nature Communications* **14**, 7134 (2023).

[27] E. Khalaf, S. Chatterjee, N. Bultinck, M. P. Zaletel, and A. Vishwanath, Charged skyrmions and topological origin of superconductivity in magic-angle graphene, *Science advances* **7**, eabf5299 (2021).

[28] J. Gonzalez and T. Stauber, Kohn-luttinger superconductivity in twisted bilayer graphene, *Physical review letters* **122**, 026801 (2019).

[29] H. C. Po, L. Zou, A. Vishwanath, and T. Senthil, Origin of mott insulating behavior and superconductivity in twisted bi-layer graphene, *Physical Review X* **8**, 031089 (2018).

[30] D. F. Agterberg, J. S. Davis, S. D. Edkins, E. Fradkin, D. J. Van Harlingen, S. A. Kivelson, P. A. Lee, L. Radzihovsky, J. M. Tranquada, and Y. Wang, The physics of pair-density waves: cuprate superconductors and beyond, *Annual Review of Condensed Matter Physics* **11**, 231 (2020).

[31] A coexisting intervalley condensate with zero center-of-mass momentum,  $\Delta_0$ , can also couple to the PDW order to induce a secondary CDW: The charge modulation from this second mechanism has a momentum of  $2\mathbf{Q}$  and, like the first, behaves as  $\cos(2\mathbf{K} \cdot \mathbf{r})$  on the atomic scale. This will then lead to an observed Kekulé pattern in the charge channel which can be observed in STM.

[32] Rigorously, the momentum transfer involved is  $\mathbf{q} + \mathbf{G}_j$ , where  $\mathbf{q}$  lies within the first mini-Brillouin Zone and  $\mathbf{G}_j$  is a moiré reciprocal lattice vector. In the Bistritzer-MacDonald model,  $|\mathbf{G}_j|$  can be up to three or four times the magnitude of the primitive moiré reciprocal lattice vectors. Nevertheless, the total momentum  $|\mathbf{q} + \mathbf{G}_j|$  remains significantly smaller than any momentum associated with the atomic scale.

[33] This conclusion is general and applies to a large class of short-range interaction, as the argument holds if the set of nearest-neighbor vectors,  $\delta_j$ , is replaced by any short-range atomic vector and its  $C_3$  rotational partners.

[34] Y. Cao, D. Rodan-Legrain, J. M. Park, N. F. Q. Yuan, K. Watanabe, T. Taniguchi, R. M. Fernandes, L. Fu, and P. Jarillo-Herrero, Nematicity and competing orders in superconducting magic-angle graphene, *Science* **372**, 264 (2021).

[35] J. Ahn, S. Park, and B.-J. Yang, Failure of nielsen-ninomiya theorem and fragile topology in two-dimensional systems with space-time inversion symmetry: Application to twisted bilayer graphene at magic angle, *Phys. Rev. X* **9**, 021013 (2019).

[36] H. Kim, Y. Choi, C. Lewandowski, A. Thomson, Y. Zhang, R. Polski, K. Watanabe, T. Taniguchi, J. Alicea, and S. Nadj-Perge, Evidence for unconventional superconductivity in twisted trilayer graphene, *Nature* **606**, 494 (2022).

[37] Q. Chen, Z. Wang, R. Boyack, S. Yang, and K. Levin, When superconductivity crosses over: From bcs to bec, *Reviews of Modern Physics* **96**, 025002 (2024).

[38] S. Van Loon and C. Sá de Melo, Topological two-band electron-hole superconductors with d-wave symmetry: Absence of dirac quasiparticle annihilation in magic-angle twisted trilayer graphene, *Physical Review B* **111**, 064515 (2025).

[39] Although their Bogoliubov Fermi surfaces are larger, there is some similarity here to work from Christos *et al*, *Nat. Commun.* 14, 7134 and Agterberg *et al*, *Phys. Rev. Lett.* 118, 127001.

[40] J. M. Park, S. Sun, K. Watanabe, T. Taniguchi, and P. Jarillo-Herrero, Simultaneous transport and tunneling spectroscopy of moiré graphene: Distinct observation of the superconducting gap and signatures of nodal superconductivity, *arXiv preprint arXiv:2503.16410* (2025).

[41] A. Pushp, C. V. Parker, A. N. Pasupathy, K. K. Gomes, S. Ono, J. Wen, Z. Xu, G. Gu, and A. Yazdani, Extending universal nodal excitations optimizes superconductivity in  $\text{bi}_2\text{sr}_2\text{cacu}_2\text{o}_{8+\delta}$ , *Science* **324**, 1689 (2009).

[42] T. Reber, N. Plumb, Y. Cao, Z. Sun, Q. Wang, K. McElroy, H. Iwasawa, M. Arita, J. Wen, Z. Xu, *et al.*, Preparing and the filling of the gap in the cuprates from the tomographic density of states, *Physical Review B* **87**, 060506 (2013).

[43] Z. Wang, K. Wang, and K. Levin, *Superconductivity on the edge of vanishing magnetic order* (2025), [arXiv:2506.18996 \[cond-mat.supr-con\]](https://arxiv.org/abs/2506.18996).

[44] K. Wang, Q. Chen, R. Boyack, and K. Levin, *Anomalous superfluid density in pair-density-wave superconductors* (2025),

arXiv:2506.13631 [cond-mat.supr-con].

[45] K. Hejazi, C. Liu, H. Shapourian, X. Chen, and L. Balents, Multiple topological transitions in twisted bilayer graphene near the first magic angle, *Phys. Rev. B* **99**, 035111 (2019).

[46] The small asymmetric shift  $\delta\epsilon$  appears in the argument of the hyperbolic tangent, which is negligible in the regimes considered and does not affect our conclusions.

[47] An equivalent approach is to show that the condensate is not invariant under  $C_3$ . The proof is similar.